Docking, not fusion, as the rate-limiting step in a SNARE-driven vesicle fusion assay

Elizabeth A Smith and James Carl Weisshaar

SUPPLEMENTAL MATERIAL

a.

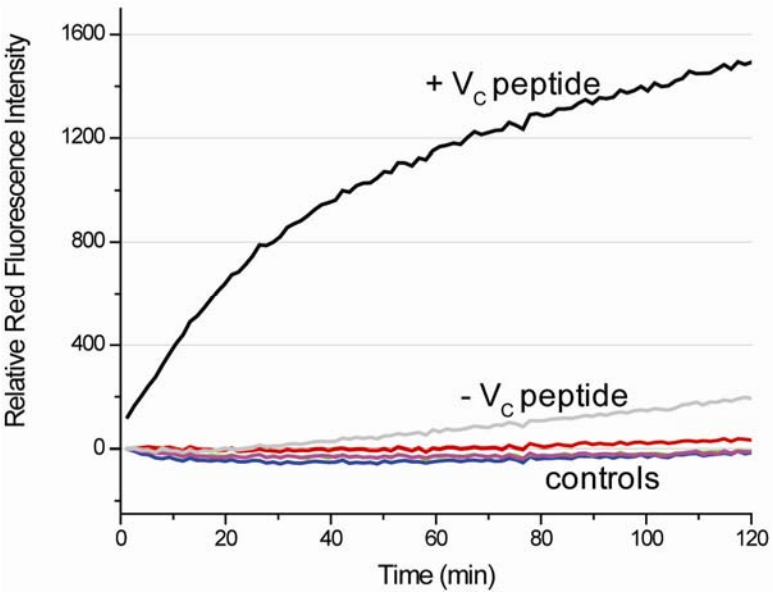

b.

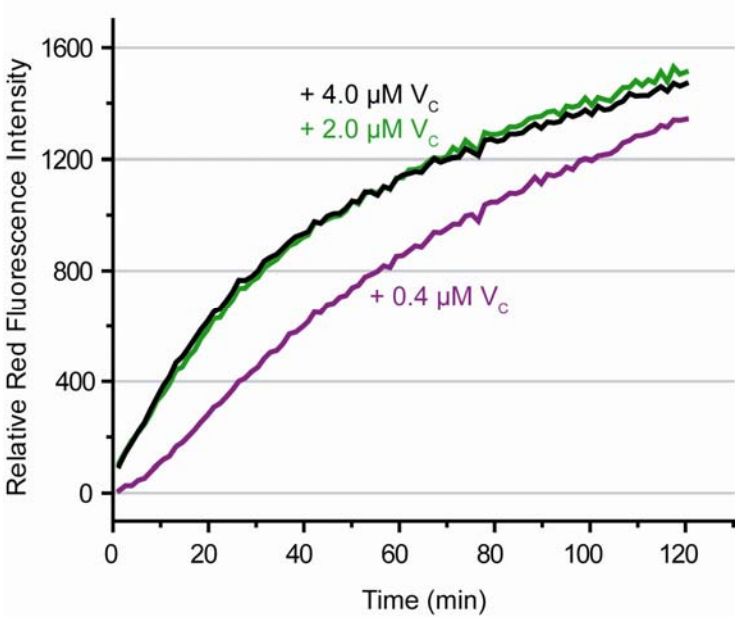

Figure S1. Bulk Lipid Mixing from FRET Assay With and Without V_C Peptide

Composite rate of vesicle-vesicle docking and fusion determined using bulk fusion assay. *a*) Red fluorescence measured during green excitation from a bulk mixture of 5 nM v-SNARE vesicles labeled with 2% DiD and 10 nM t-SNARE vesicles labeled with 2% DiI in the presence (+ V_C) and absence (–V_C) of 4 µM V_C peptide. Controls: No significant lipid mixing occurs if v-SNARE vesicles are mixed with vesicles that have one or both t-SNARE proteins removed (magenta curve: Syx only; blue curve: Protein Free) or if SNAP-25 is truncated to simulate BoNT/E cleavage (green curve: BoNT/E in the absence of V_C peptide; red curve: BoNT/E in the presence of V_C peptide). *b*) Optimization of V_C peptide concentration by measurement of red fluorescence during green excitation from a bulk mixture of 5 nM v-SNARE vesicles labeled with 2% DiD and 10 nM t-SNARE vesicles labeled with 2% DiI. Bulk lipid

mixing was enhanced comparably at 2 μM (green curve) and 4 μM V_C peptide (black curve) and much less so at 0.5 μM V_C peptide (purple curve).

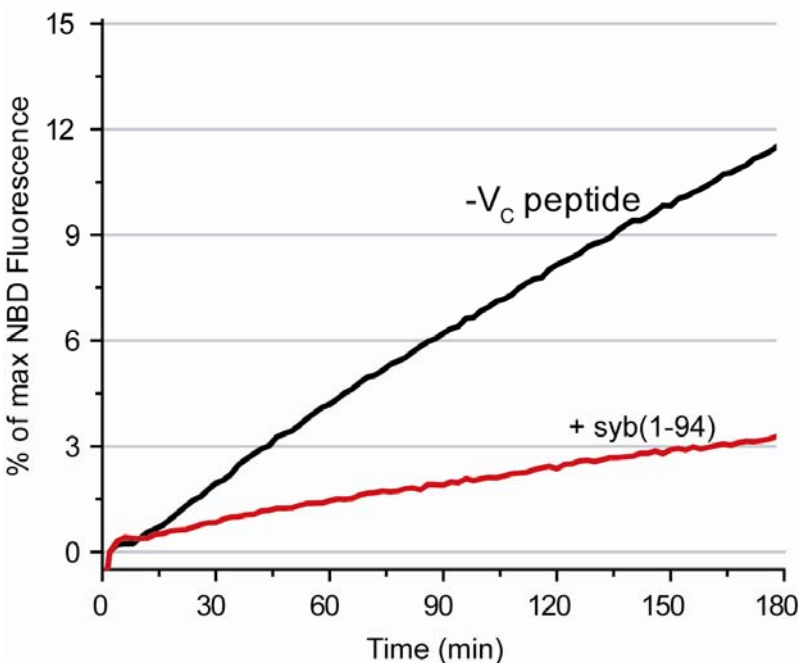

Figure S2. Bulk Lipid Mixing Assay from NBD Dequenching

Assay carried out using the dequenching method of Weber *et al*. (1). The v-SNARE vesicles were reconstituted with 1.5% NBD-PE and 1.5% Rhodamine-PE and t-SNARE vesicles were unlabeled. The extent of lipid mixing was monitored by NBD fluorescence, which is largely quenched in the absence of fusion due to efficient FRET from NBD to Rhodamine. Vesicles were mixed at a 9:1 t-SNARE vesicle: v-SNARE vesicle ratio with t-SNARE vesicles at 60 nM (black curve). The rate of lipid mixing slows in the presence of 10 μM syb(1-94) (red curve).

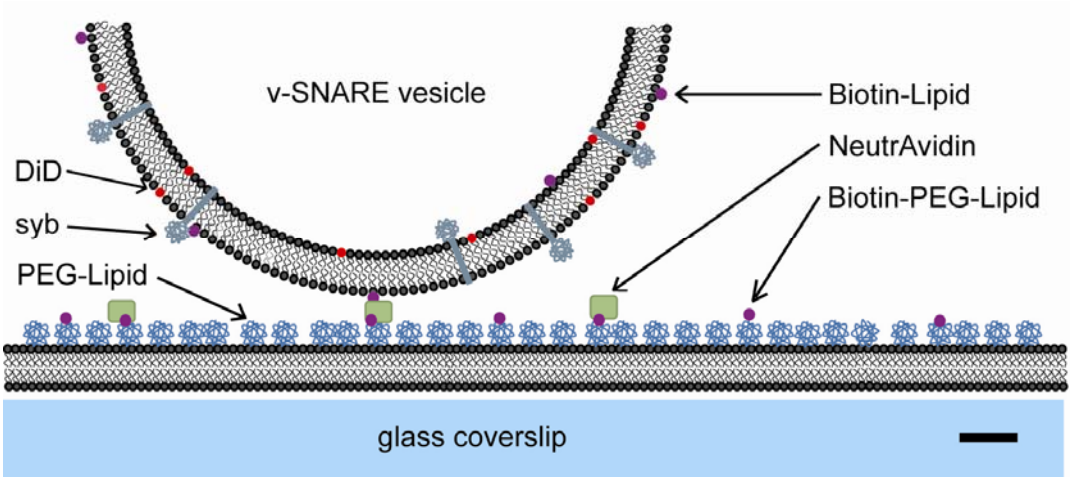

Figure S3. Schematic of Vesicle Tethering Method

The v-SNARE vesicles are tethered via biotin-NeutrAvidin interactions to a PEG-functionalized lipid bilayer supported on glass. The v-SNARE vesicle membrane contains 0.2% biotin-PE and the supported lipid bilayer contains 1% biotin-PEG-DPPE. Scale bar = 5 nm.

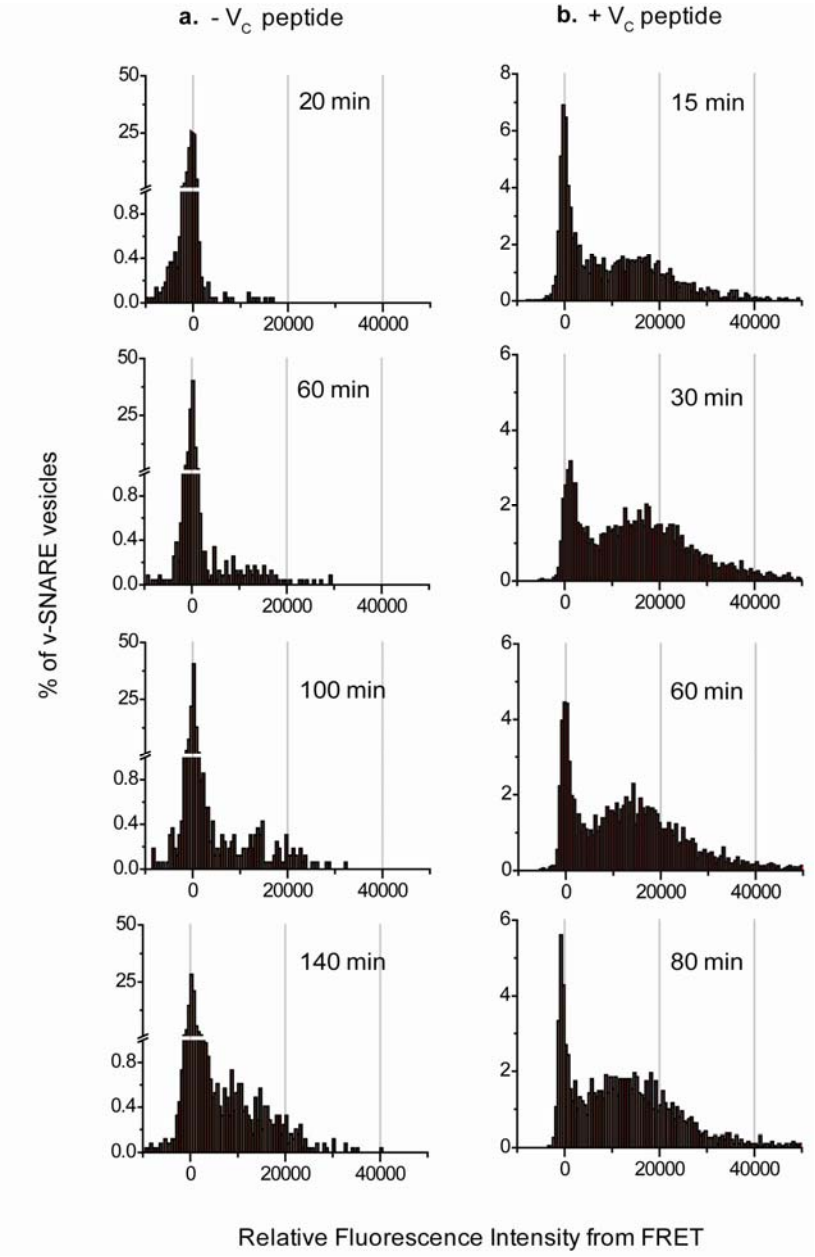

Figure S4. Histograms of FRET Intensity for Single, Tethered v-SNARE Vesicles

Tethered DiD-labeled v-SNARE vesicles were incubated with 10 nM DiI-labeled t-SNARE vesicles for: *a*) 20, 60, 100, and 140 min in the absence of V_C peptide and *b*) 15, 30, 60 and 80 min in the presence of 5 μM V_C peptide. At the specified reaction time, excess t-SNARE vesicles were rinsed away and the surface was imaged over several fields of view for up to 5 min using alternating laser excitation. The fluorescence intensity due to FRET from DiI to DiD, I_{FRET}^{514}, was determined for each v-SNARE vesicle after correcting for two sources of cross-talk (Eq. S1). The FRET intensity values are presented in the histograms, which are normalized to account for variations in the number of v-SNARE vesicles imaged at each reaction interval. The large peak centered at zero reflects the population of v-SNARE vesicles that have not docked with a t-SNARE vesicle, that have docked with a t-SNARE vesicle without measurable FRET, or that are experiencing a "false co-localization". Inclusion of V_C peptide enhances the fraction of v-SNARE vesicles that undergo FRET after a given reaction time.

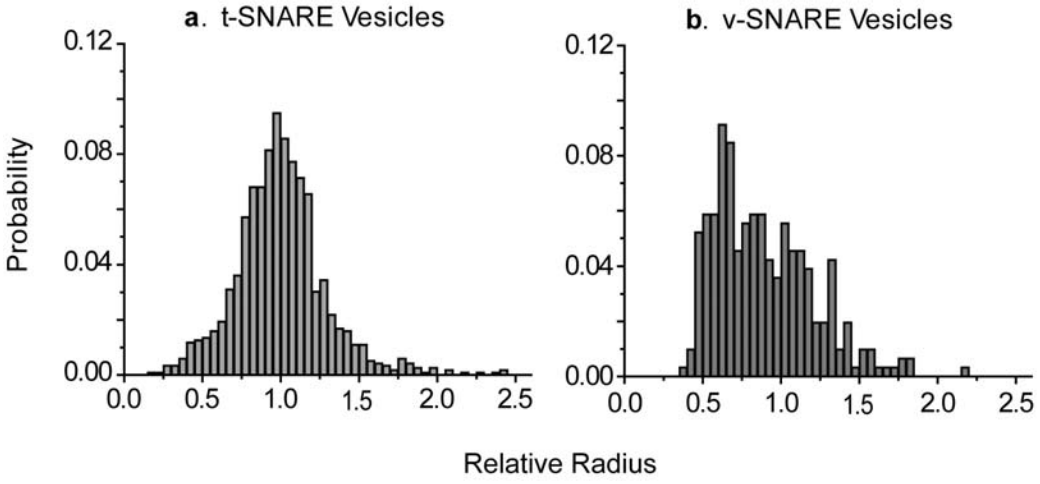

Figure S5. Relative Size Distribution of v-SNARE and t-SNARE Vesicles

The relative radius of each vesicle was determined from the square-root of its background-corrected fluorescence intensity. Histograms show the relative radii of the entire population of *a*) DiI-labeled t-SNARE vesicles and *b*) DiD-labeled v-SNARE vesicles. The two histograms were placed on the same relative scale after correcting for differences in excitation and emission efficiencies of the labels (Supplemental Methods). Electron microscopy of similarly prepared vesicles found that the t- and v-SNARE vesicles have a mean radius of 33 nm and 39 nm, respectively, and that both v- and t-SNARE vesicle radii range from 15-75 nm. (Personal communication from Enfu Hui and Ed Chapman, UW-Madison Dept. of Physiology).

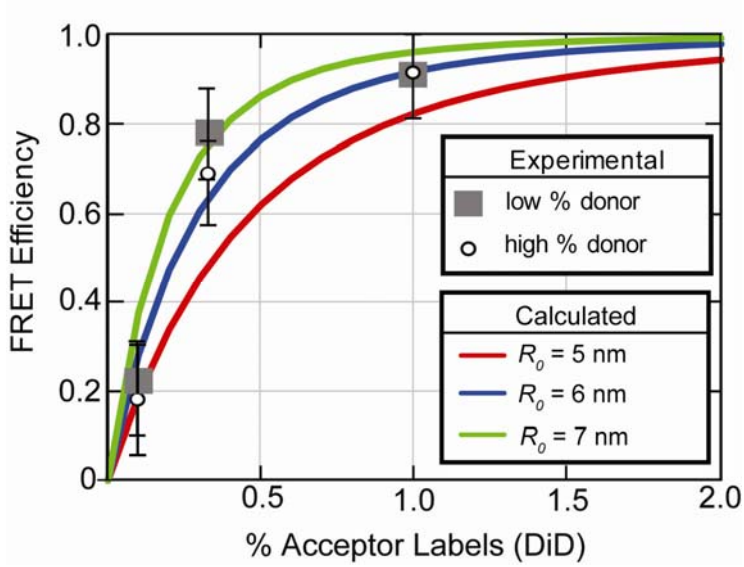

Figure S6. **FRET Efficiencies of Mixed Vesicles**

To simulate full fusion between different-sized v-SNARE and t-SNARE vesicles, mixed-label vesicles were reconstituted with varying fraction of DiI (donor) and DiD (acceptor) labels. The mixed vesicles were immobilized on glass and the FRET efficiency from DiI to DiD was measured (Eq. S2). Three different acceptor fractions were used, each at two different donor fractions. Specifically, the "high % donor" mixtures (open circles) were: 0.1% DiD + 1.9% DiI, 0.33% DiD + 1.67% DiI, and 1% DiD + 1% DiI. The "low % donor" mixtures (gray squares) were: 0.1% DiD + 0.48% DiI, 0.33% DiD + 0.42% DiI, and 1% DiD + 0.25% DiI. Smooth curves are the calculated FRET efficiency vs % Acceptor labels for our model of fully fused vesicles. The model calculates FRET efficiency for a randomly distributed mixture of donor and acceptor labels lying in two parallel planes spaced by 4 nm. Three different Förster radii were tested: R_0 = 5 nm (red line), 6 nm (blue line), and 7 nm (green line). See Supplemental Data for details.

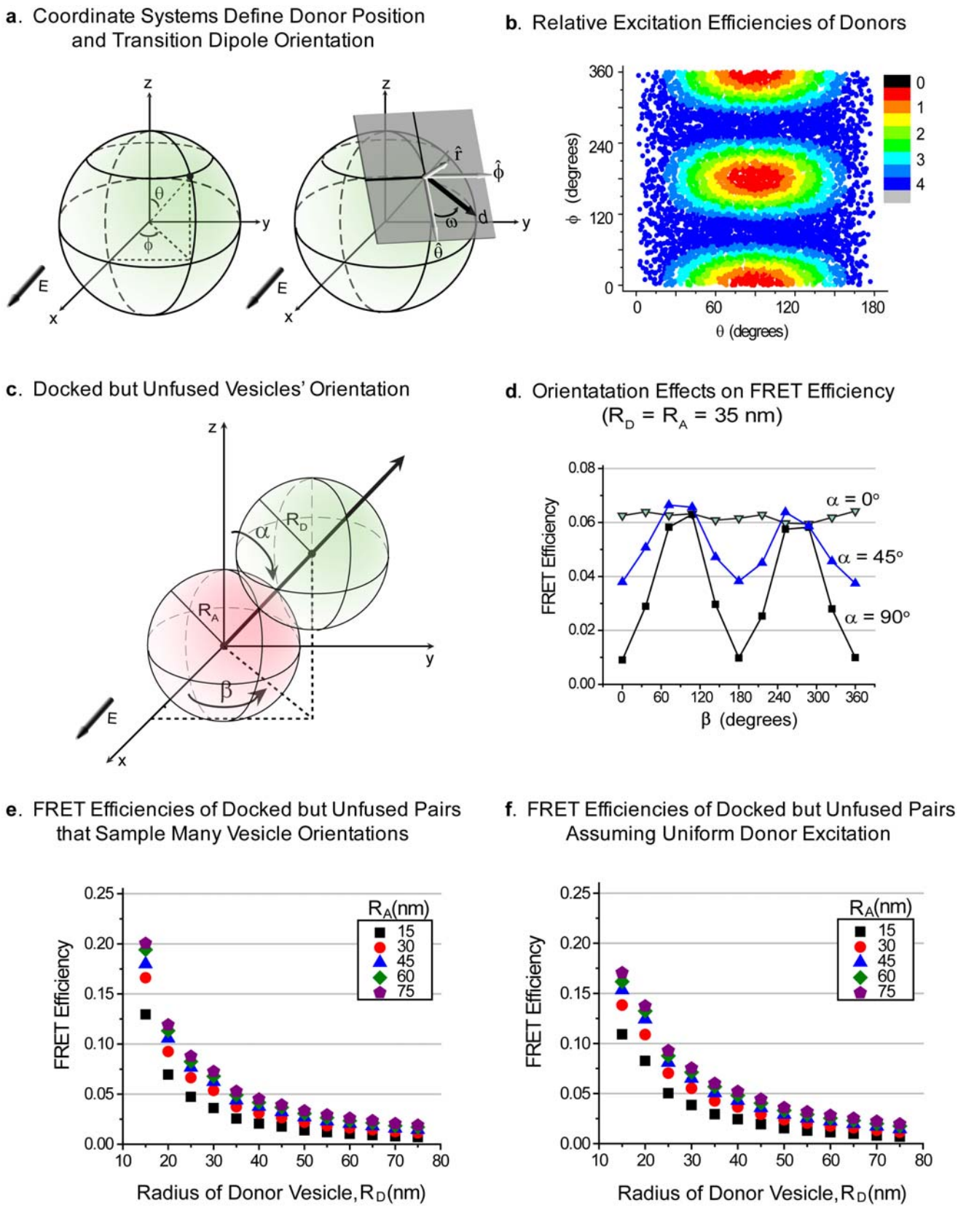

Figure S7. **Model Estimates of FRET Efficiency for Docked but Unfused Vesicle Pairs**

Docked but unfused vesicle pairs are modeled as a pair of touching spheres. Each sphere has two surfaces (lipid bilayer leaflets) that are separated by 4 nm and decorated with a random distribution of labels. The donor labels are excited with an s-polarized evanescent wave whose electric-field vector ***E***

points in the x-direction in the Cartesian (xyz) coordinate system; the glass coverslip in the experiment lies in the xy-plane. *a*) The position of a donor label on the surface of the sphere is specified in spherical polar coordinates by its polar angle θ and azimuthal angle ϕ. Originating from its position are three local, mutually orthogonal unit vectors $\hat{\boldsymbol{r}}$, $\hat{\boldsymbol{\theta}}$, and $\hat{\boldsymbol{\phi}}$ that point in the direction of increasing r, θ, and ϕ, respectively. The donor transition dipole moment vector $\boldsymbol{d}$ lies tangent to the surface of the sphere. Its projections along $\hat{\boldsymbol{\theta}}$ and $\hat{\boldsymbol{\phi}}$ are determined by the angle between $\boldsymbol{d}$ and $\hat{\boldsymbol{\theta}}$, which we call ω. In the FRET calculations, ω is assumed to be uniformly distributed in the $\theta\phi$-plane. See Supplemental Data for details. *b*) Color map indicating donor relative excitation efficiencies according to the (θ, ϕ) location on the sphere. Labels whose transition dipoles on average lie more nearly parallel to the electric vector $\boldsymbol{E}$ (at the vesicle "poles", for example) are excited more efficiently than those that lie on average more perpendicular to $\boldsymbol{E}$. *c*) The orientation of a docked but unfused vesicle pair is defined by a vector that connects the two vesicle centers. The orientation of this vector is specified a polar angle α and azimuthal angle β. *d*) Calculated FRET efficiency for a model pair of 35-nm radius vesicles that are docked but unfused using R_0 = 6 nm. FRET efficiency is plotted vs β for the values α = 0º, 45º, 90º. *e*) The mean FRET efficiency for a docked but unfused vesicle pair with donor radius R_D and acceptor radius R_A that samples different values of α and β. Effects of laser polarization on excitation efficiency are included. See Supplemental Data for details. *f*) Same as in panel *e*, except that all donors are excited with equal efficiency (no polarization effects).

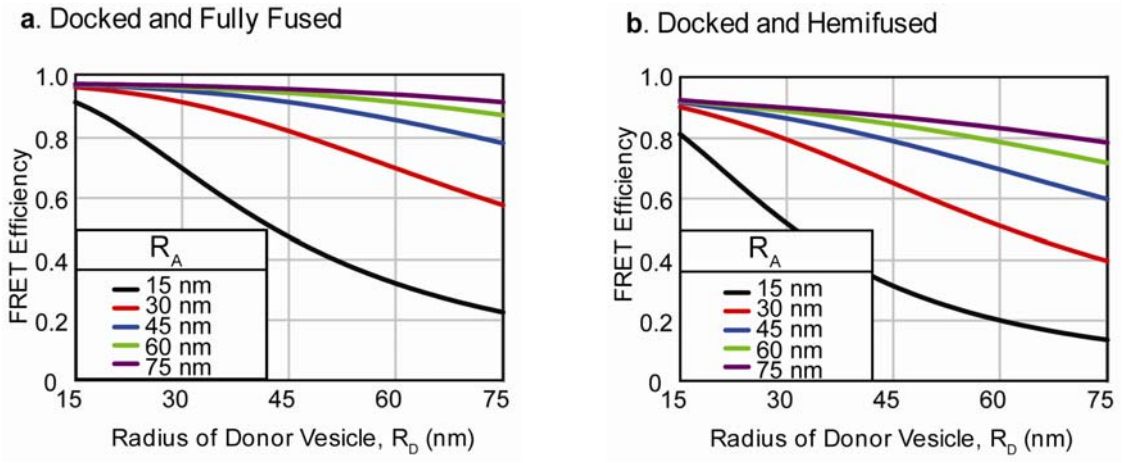

Figure S8. Model Estimates of Docked and Fused FRET Efficiency *E*

a) Docked and fully fused vesicles were modeled as one pair of parallel planes ("lipid bilayer leaflets") that each contains a random distribution of donor and acceptor labels. The FRET efficiency E depends on the final acceptor labeling fraction and the Förster radius. We fixed the final acceptor concentration from the ratio of donor to acceptor vesicle surface areas (assuming spherical geometries). Plotted is E vs donor vesicle radius for a number of different acceptor radii using R_0 = 6 nm. *b*) Docked and hemifused vesicles were modeled as two separate pairs of parallel planes (no inter-vesicle FRET). The hemifused donor "vesicle" is modeled as one plane containing 2% donor labels and one mixed plane (containing both donors and acceptors). The hemifused acceptor "vesicle" is modeled as one plane containing 2% acceptor labels and one mixed plane. The labeling fractions of the mixed plane were the same for both vesicles and determined from the ratio of the outer leaflet surface areas of the vesicle pair. The FRET efficiency was calculated for each plane using R_0 = 6 nm. Plotted is the weighted average of FRET efficiency for each plane, with the weights reflecting the relative concentration of donor labels. See Supplemental Data for details.

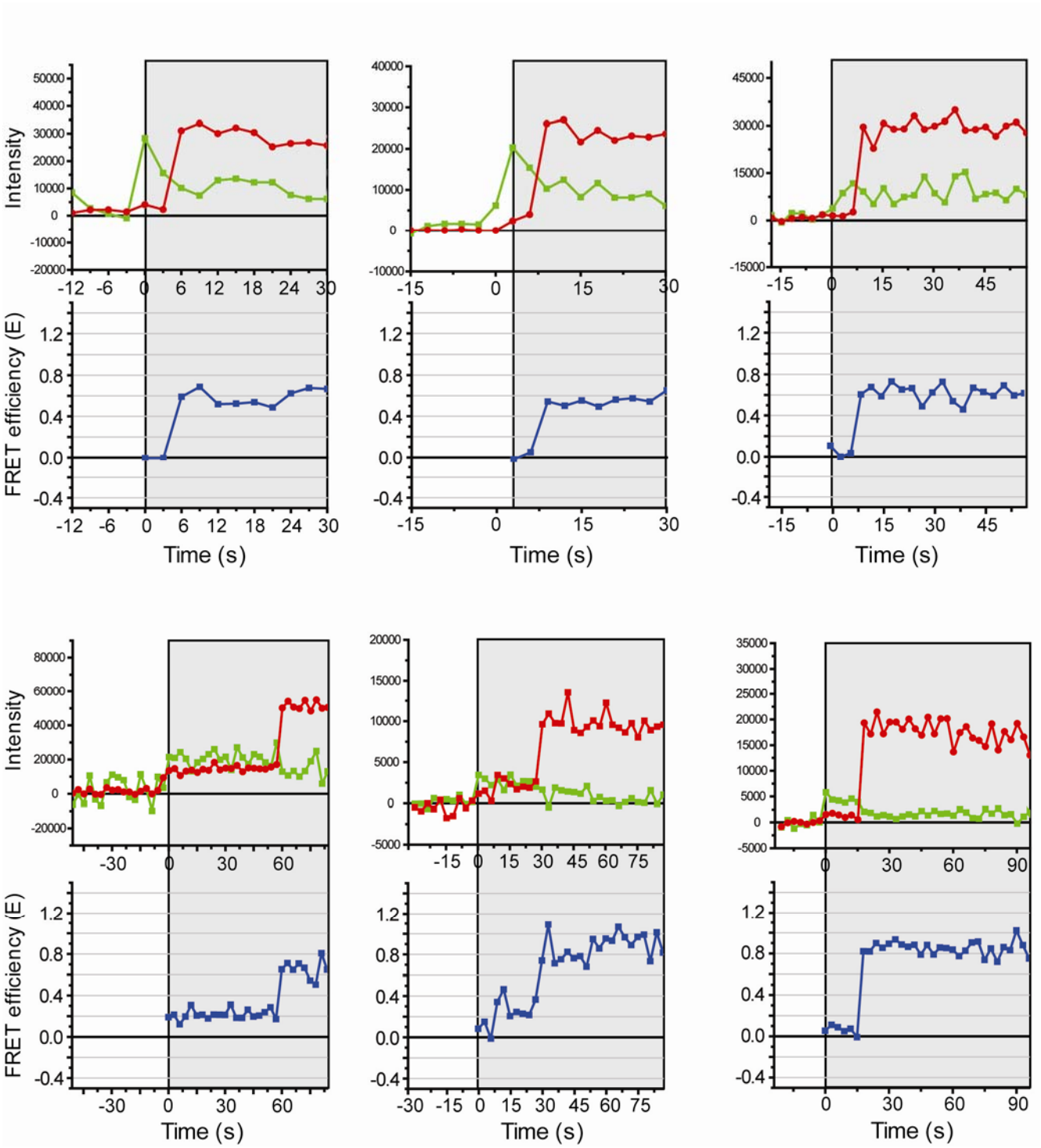

Figure S9. Intensity and FRET Efficiency Traces of Individual Docking and Fusion Events.

Background-subtracted, integrated green and red intensities during 514 nm excitation for six well-isolated docking and fusion events observed with 3-s time resolution. Visual inspection of the movie determined the time during which the vesicles were stably co-localized (indicated by gray shading). The corresponding absolute FRET efficiency E (Eq. S2) of the vesicle pair is plotted in blue below the intensity traces. When the vesicles first co-localize the FRET efficiency is low, $E = 0 – 0.25$. The pair then makes an abrupt transition to a high FRET state, $E = 0.5 – 0.95$. For several fusion events, we did not observe a low-FRET state. We interpret these as fast fusion events with $\tau_{fus} < 3$ s.

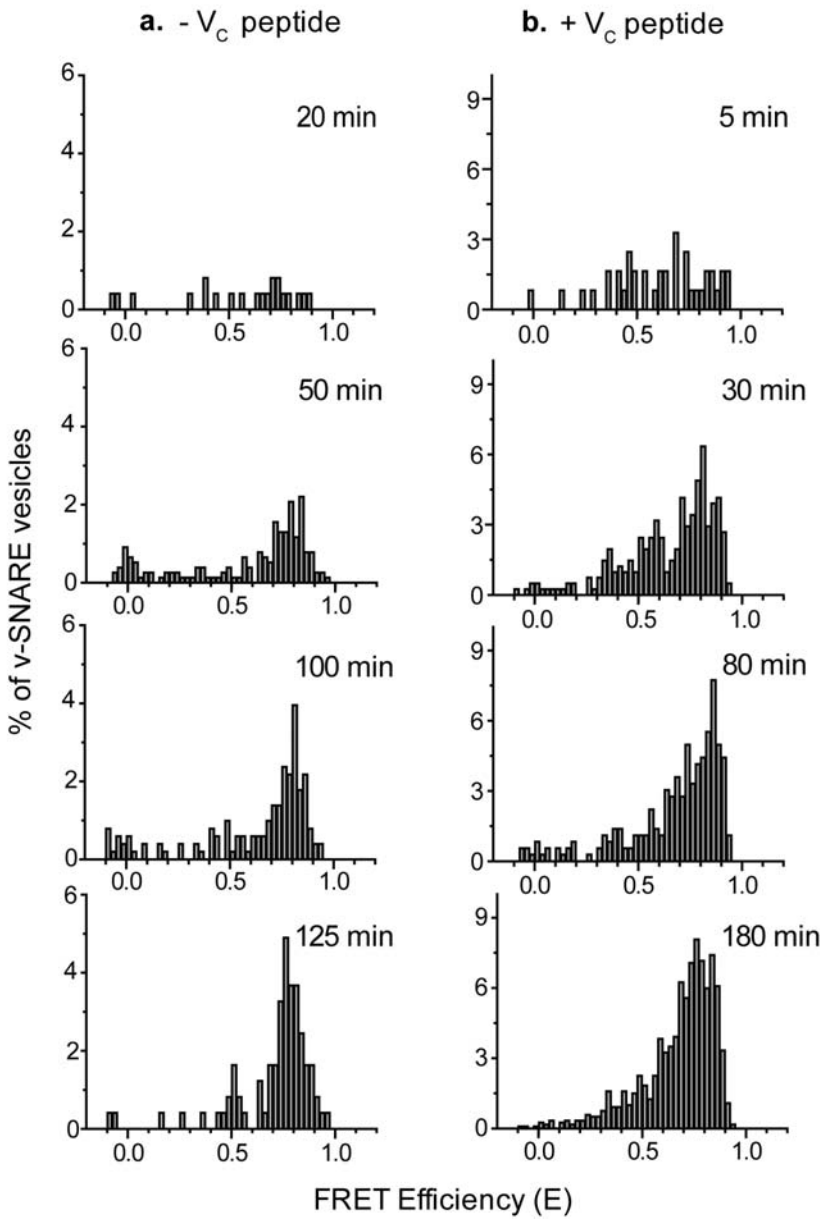

Figure S10. FRET Efficiency Histograms for Bulk Fusion Assay vs Reaction Time

10 nM t-SNARE vesicles labeled with 2% DiI were mixed with 5 nM v-SNARE vesicles labeled with 2% DiD *a*) without V_C peptide or *b*) in the presence of 5 μM V_C peptide. At the specified reaction times, the vesicle mixture was sampled, diluted, and plated onto glass for FRET analysis of co-localized v-SNARE/t-SNARE vesicle pairs. FRET efficiency histograms are normalized to account for variations in the total number of v-SNARE vesicles examined at each time point.

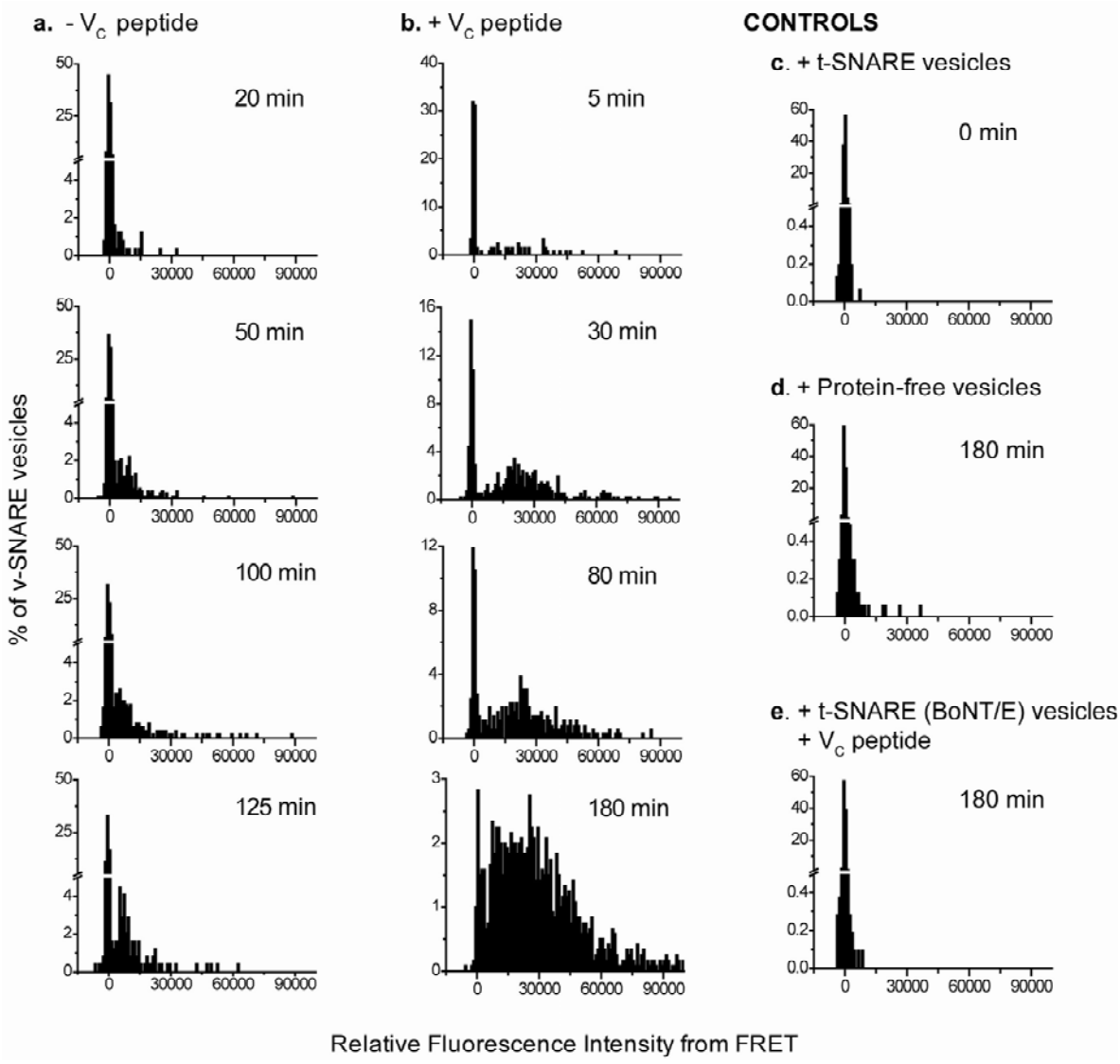

Figure S11. Histograms of FRET Intensity for Single v-SNARE Vesicles from Bulk Fusion Assay

5 nM v-SNARE vesicles labeled with 2% DiD were mixed with 10 nM t-SNARE vesicles labeled with 2% DiI *a*) without V_C peptide or *b*) in the presence of 5 μM V_C peptide. At the specified reaction time, the vesicle mixture was sampled, immobilized on glass, and imaged over several fields of view for up to 10 min. Fluorescence intensity due to FRET from DiI to DiD, I_{FRET}^{514}, was determined for each v-SNARE vesicle after correcting for two sources of cross-talk (Eq. S1). The histograms are normalized to account for variations in the number of v-SNARE vesicles imaged at each reaction interval. In each histogram the peak centered at zero reflects the population of v-SNARE vesicles that have not yet docked with a t-SNARE vesicle, that have docked with a t-SNARE vesicle without measurable FRET, or that are experiencing a false co-localization. Inclusion of V_C peptide greatly enhances the fraction of v-SNARE vesicles that undergo FRET after a given reaction time. *Controls*: *c*) v-SNARE vesicles were immobilized sparsely onto a glass coverslip. The coverslip was thoroughly rinsed and then t-SNARE vesicles were immobilized sparsely onto the same glass coverslip. *d*) 5 nM v-SNARE vesicles were mixed with 10 nM protein free vesicles labeled with 2% DiI for 180 min, sampled, and immobilized on glass. *e*) 5 nM v-SNARE vesicles were mixed with 5 μM V_C peptide and 10 nM 2% DiI-labeled t-SNARE vesicles designed to mimic BoNT/E cleavage for 180 min, sampled, and immobilized on glass.

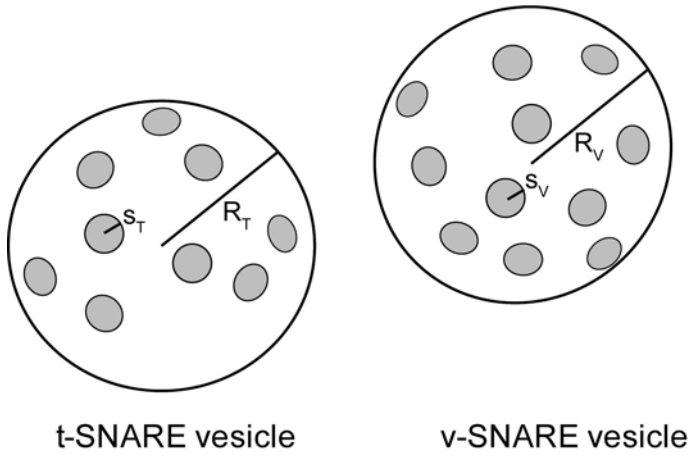

Figure S12. Collision Encounter Model

The v-SNARE and t-SNARE vesicles are modeled as spheres of equal size. The SNARE proteins were modeled as absorbing disks that occupy a fraction of the surface area. The absorbing disks on both v-SNARE and t-SNARE vesicles have a radius of 2 nm. There are 45 disks on the v-SNARE vesicle and 65 disks on the t-SNARE vesicle.

Movie S1. A Single Docking and Fusion Event with 3 s Time Resolution

The left half of the movie shows fluorescence detected in the green channel and the right half of the movie shows fluorescence detected in the red channel at the same position in space during excitation at 514 nm. At t = 0, a green fluorescent, DiI-labeled t-SNARE vesicle adsorbs from solution and co-localizes with a tethered v-SNARE vesicle. The position of the tethered v-SNARE vesicle labeled by red-fluorescent DiD was confirmed using 633 nm excitation (not shown). The t-SNARE vesicle remains co-localized without significant FRET (docked but unfused) with the v-SNARE vesicle for two frames. By the third frame the green fluorescence has disappeared simultaneous with the appearance of fluorescence in the red channel due to FRET. The delay between docking and fusion is τ_{fus} = 6 s for this particular event.

SUPPLEMENTAL METHODS

Preparation of Proteoliposomes

Recombinant neuronal SNARE proteins were expressed and purified from bacteria. A detailed description of the plasmids, cell lines, buffers, and procedures used has been given previously (2). The specific proteins used were the full-length, wild type v-SNARE protein mouse synaptobrevin-2 His_6 (syb) and rat His_6 syntaxin-1A (syx); a binary t-SNARE complex composed of syx and mouse His_6 SNAP-25B; and a binary t-SNARE complex composed of syx and a truncated version of mouse His_6 SNAP-25B (syx + SNAP-25Δ26), which was designed to correspond to the SNAP-25 fragment that would be left following cleavage with *Clostridium botulism* neurotoxin serotype E (BoNT/E) (2). Both t-SNARE heterodimers were co-expressed from a dicistronic vector in bacteria, then purified and reconstituted simultaneously into vesicles. A peptide derived from the C-terminus of syb (aa 57- 92, the V_C peptide) was synthesized by the University of Wisconsin-Madison Biotechnology Center. The peptide was purified with high-pressure liquid chromatography to ~80% purity.

The t-SNARE and v-SNARE proteins were reconstituted by the co-micellization method into proteoliposomes, as described in detail previously (3). The lipid content is 55% (mol/mol) 1-palmitoyl, 2-oleoyl phosphatidylcholine (POPC), 15% 1,2-dioleoyl phosphatidylserine (DOPS) and 28% 1,2-dioleoyl phosphatidylethanolamine (DOPE). The v-SNARE vesicles are labeled with 2% 1,1'-dioctadecyl-3,3,3',3'-tetramethylindodicarbocyanine, 4-chlorobenzenesulfonate (DiD) and 0.2% 1,2-dipalmitoyl-*sn*-glycero-3-phosphoethanolamine-N-(biotinyl) (biotin PE); t-SNARE vesicles are labeled with 2% 1,1'-dioctadecyl-3,3,3',3'-tetramethylindocarbocyanine perchlorate (DiI). All synthetic phospholipids were purchased from Avanti Polar Lipids (Alabaster, AL). Fluorescent labels were purchased from Molecular Probes (Eugene, OR).

Proteoliposomes were purified away from unincorporated lipids, detergent, and proteins by flotation in an Accudenz (Accurate Chemical, Westbury, NY) step gradient. Protein incorporation was confirmed by sodium dodecyl sulfate polyacrylamide gel electrophoresis (SDS-PAGE). To remove Accudenz from the fusion experiments, purified t-SNARE vesicles were put into dialysis membranes (Spectra/Por 6-8,000 molecular weight cutoff, Spectrum Laboratories, Inc. Rancho Dominguez, CA) and dialyzed overnight against 25 mM HEPES·KOH, 100 mM KCl, 10% glycerol, and 1 mM dithiothreitol (pH 7.40) (all salts from Sigma-Aldrich) at 4 ^{o}C. Assuming similar protein and lipid recovery as measured directly by Tucker et al. (2), purified donor vesicles have ~95 total t-SNARE/syx + SNAP-25Δ26/ syx (~65 "correctly oriented") copies per vesicle and were harvested at 2.7 mM lipid (assuming the average vesicle contains 27,000 lipids, this corresponds to 100 nM vesicles). Acceptor vesicles have ~60 syb (~45 "correctly oriented") copies per vesicle on average. It is possible that the protein copy number is highly variable from vesicle to vesicle (4). The vesicles were used fresh or flash-frozen in liquid Nitrogen and stored at -80 ^{o}C.

Bulk Fusion Experiments

We carried out bulk vesicle fusion experiments presented in Fig. S1*a,b* in 96-well FluoroNunc plates (Nunc/Thermo Fisher Scientific, Rochester, NY). Each well of the microplate contained 125 μL total volume, including 5 nM DiD-labeled v-SNARE vesicles and 10 nM DiI-labeled t-SNARE vesicles in Fusion Buffer (25 mM HEPES·KOH, 100 mM KCl, 0.2 mM EGTA, and 1 mM dithiothreitol, pH 7.40). Lipid mixing was observed as an increase in FRET from DiI labels, which were reconstituted into t-SNARE vesicle membranes, to DiD labels, which were reconstituted into v-SNARE vesicle membranes, by measuring DiD (acceptor) fluorescence at 700 ± 4.5 nm during DiI (donor) excitation at 514 ± 4.5 nm using a microplate reader (Molecular Devices SpectraMAX Gemini, Sunnyvale, CA). For the control experiments shown in Fig. S1*a*, the exact volume of DiI-labeled control vesicles (protein free, BoNT/E cleavage simulation, syx only) was adjusted such that each sample had a constant absorbance at 514 nm (Varian Cary 50 UV/Vis Spectrophotometer, Palo Alto, CA). The vesicles were pre-warmed to 37^{o}C prior to mixing.

The bulk vesicle-vesicle fusion experiment shown in Fig. S2 used vesicles prepared identically to the DiD- and DiI-labeled vesicles. The only difference was that the v-SNARE vesicles were reconstituted to include 1.5% N-(7-nitro-2-1,3-benzoxadiazol-4-yl)-1,2-dipalmitoyl phosphatidylethanolamine (NBD-PE) and 1.5% N-(lissamine rhodamine B sulfonyl)-1,2-dipalmitoyl phosphatidylethanolamine (Rhodamine-PE) and the t-SNARE vesicles were unlabeled. Lipid mixing was monitored by measuring NBD fluorescence at 530 ± 10 nm during excitation at 460 ± 20 nm using a microplate reader (BioTek Synergy HT, Winooski, VT). The vesicles were pre-warmed separately to 37^{o}C prior to mixing at a 1:9 v-SNARE vesicle: t-SNARE vesicle ratio in a 96-well FluoroNunc plate (Nunc/Thermo Fisher Scientific, Rochester, NY). The total volume was 75 μL, including 6.7 nM v-SNARE vesicles and 60 nM t-SNARE vesicles in Fusion Buffer. Fusion between the doubly-labeled v-SNARE vesicles and unlabeled t-SNARE vesicles caused the average distance between NBD and Rhodamine labels to increase, which decreased the efficiency of NBD FRET to Rhodamine and therefore increased NBD's fluorescence quantum yield. After three hours of incubation time 20 μL of *n*-dodecyl-β-D-maltoside was injected into the solution to a final concentration of 0.5% w/v. NBD fluorescence is plotted as a function of time in Fig. S2 by subtracting the initial fluorescence intensity

value and then normalizing the fluorescence signal to the maximum NBD fluorescence measured after detergent addition. Lipid mixing between 6.7 nM v-SNARE vesicles and 60 nM t-SNARE vesicles was also assayed in the presence of 10 μM of the cytoplasmic domain of syb (aa 1-94).

Tethering of v-SNARE vesicles to a PEG-Functionalized Supported Lipid Bilayer

The single-vesicle fusion assay requires one vesicle type (here the v-SNARE vesicles) to be tethered to a passivated glass surface. To form the passivating layer, protein-free liposomes composed of 80% POPC, 15% DOPS, and either 5% 1,2-distearoyl-*sn*-glycero-3-phosphoethanolamine-N-[methoxy(polyethylene glycol)-2000] (PEG) or 5% 1,2-distearoyl-*sn*-glycero-3-phosphoethanolamine-N-[biotinyl(polyethylene glycol)-2000] (Biotin-PEG) were prepared using the same reconstitution and purification procedure as used for the SNARE-bearing vesicles. Purified vesicles were introduced above a clean, hydrophilic glass coverslip (Fisherfinest Premium Cover Glasses, Fisher Scientific, Waltham, MA) where they spontaneously formed a supported lipid bilayer (SLB).

Supported lipid bilayers for use in the tethered vesicle fusion experiments were nearly free of defects that cause non-specific binding of v-SNARE and t- SNARE vesicles. Typically, the bilayers used for these experiments had <5 defects per 6400 μm^2 of surface area, as was assayed frequently by introducing a dilute solution of vesicles above the bilayer. Bilayers of sufficient quality were achieved by depositing the vesicles at a low temperature using a protocol developed previously in our lab (5). A 4:1 mixture of PEG: biotin-PEG vesicles were diluted a factor of 100 (~30 μM total lipid) in Membrane-Making Buffer (MMB; 25 mM HEPES·KOH and 100 mM KCl, pH 7.40). Fresh MMB was made frequently and filtered using 0.22 μm pore cellulose acetate membranes (Corning Life Sciences, Lowell, MA).The vesicles were deposited into the sample cells at room temperature, stored in a covered glass dish, and immediately placed into a 4°C refrigerator. After ≥ 2.5 hr, the glass dish was moved to a 37°C incubator (Model 1525, VWR International, West Chester, PA) for ≥ 4 hr. The bilayers could be stored at 4°C overnight or in the 37°C incubator for up to ~5 hr, provided they did not dry out. A clean glass coverslip served as the bottom face and "window" into our homemade sample cell. Coverslips were cleaned by sonication in a ~20% v/v detergent solution (Contrad-70, Decon Labs Inc, King of Prussia, PA), rinsed extensively using 18.2 MΩ·cm Millipore water (Millipore Simplicity system, Billerica, MA), etched for 1 hour at 90°C by incubation in a commercial mixture of sulfuric acid and hydrogen peroxide (Nanostrip, Cyantek, Billerica, MA), and then again rinsed extensively with Millipore water before use.

Unfused PEG/Biotin-PEG vesicles were rinsed away from supported lipid bilayers by flushing each sample cell with 2 mL of 37°C MMB while the sample cells were kept at 37˚C within a modified benchtop drybath. To tether the v-SNARE vesicles, a 0.2 mg/mL solution of NeutrAvidin biotin-binding protein (ImmunoPure, Pierce, Rockford, IL) in MMB was incubated with the bilayer for 3 min then rinsed away with 3 mL of MMB. An optimal density of ~200 tethered vesicles per 3000 μm^2 surface area was achieved by first diluting the purified v-SNARE vesicles 25 times in MMB and then incubating the vesicle solution with the NeutrAvidin-functionalized surface for 20 min. After 20 min, excess v-SNARE vesicles were rinsed away using 2 mL MMB. The number of t-SNARE vesicles that non-specifically bind to the surface increased a factor of ~10-100 after functionalization with NeutrAvidin.

Most tethered v-SNARE vesicles undergo free two-dimensional diffusion. Single-particle tracking measurements on a highly mobile surface gave a diffusion constant of ~0.05 $\mu m^2/s$ with an immobile fraction of ~20%. The friction limiting the diffusion constant is likely due to polymer-polymer and NeutrAvidin-NeutrAvidin lateral interactions. The distribution of tethered vesicle diffusion coefficients and the fraction of vesicles which were immobile varied from membrane to membrane, but the v-SNARE vesicles had very similar docking and fusion kinetics regardless of their mobility.

Total Internal Reflection Fluorescence Microscopy

A modified commercial wide-field microscope (Eclipse TE2000-U, Nikon, Melville, NY) enabled selective excitation of fluorophores within ~200 nm of the glass/water interface using "through-the-objective" total internal reflection (TIR) (3). A 60×, 1.45 NA, oil-immersion objective (Olympus,

Melville, NY) combined with the Nikon tube lens made the effective magnification of the microscope 90×.

Total internal reflection of lasers at 633 nm (HeNe, Coherent, Santa Clara, CA) and 514 nm (Ar^+, Melles Griot, Carlsbad, CA) excited DiD and DiI, respectively. The evanescent wave generated by the 514 nm laser was >93% s-polarized. The two laser beams were combined using a 45° green reflective dichroic filter, (J47-268, Edmund Optics, Barrington, NJ) and then expanded together using a pair of achromatic lenses (Edmunds Optics, Barrington, NJ). Clipping the expanded laser beams using a rectangular slit prior to focusing onto the back focal plane of the objective created a rectangular region of excitation covering half of the field of view of the CCD camera. A dual band dichroic mirror 514/633PC (Chroma, Rockingham, VT) reflected the co-aligned laser beams and passed the fluorescence emission from both dyes. At the sample, the excitation intensity profile was flat to within 20% of the maximum value; the ratio of 633 nm to 514 nm intensity was constant to within 5% over the entire field of view.

Fluorescence was collected by the microscope objective, focused by the tube lens, and then collimated with an achromatic lens within a home-built dual-imaging chamber (6). A dichroic mirror reflecting 565-615 nm and passing longer wavelengths (Chroma) separated the fluorescence into "green" and "red" channels that passed emission filters HQ590/50M and HQ700/75M (Chroma), respectively. A positive lens with a long focal length was placed in the red channel such that both channels focused at the same plane. An identical dichroic mirror recombined the two channels and an achromatic lens focused them side-by-side onto an electron-multiplying charge-coupled device camera (EMCCD, Model DV897-UVB, Andor Technologies, Belfast, Northern Ireland). The camera had 16 × 16 μm^2 pixels, which corresponded to 178 × 178 nm^2 at the sample. Data acquisition was controlled through Andor Solis software (Andor Technologies). The mapping between the red and green channels was determined on a daily basis by imaging immobilized t-SNARE vesicles, which fluoresce in both channels at high laser power. The mapping function includes translation, rotation, and scaling; it maps a position in the red channel to the corresponding position in the green channel with an average deviation of 1.0 ± 0.5 pixels from the observed peak positions.

Single-Vesicle FRET Measurements

FRET efficiencies for isolated pairs of vesicles were determined from two dual-color, 50 ms camera exposures obtained in rapid succession using alternating laser excitation (ALEX) (7). The first exposure used 1.4 W/cm^2 of 633 nm excitation and the second used 1.4 W/cm^2 of 514 nm excitation. The alternation period for the lasers was 100 ms and the duty cycle was 45-48%. The timing of the lasers was controlled using mechanical shutters (Model LS2Z2, Uniblitz, Rochester, NY), which opened with a time constant of < 1 ms in response to a pulse from the camera. While imaging tethered vesicles using ALEX, the frame rate is fast enough to essentially freeze vesicle motion during both measurements. The root-mean-square displacement of a tethered vesicle is estimated as $\sqrt{4D_{ves}\tau}$ = 0.1 μm, where $D_{ves} \sim 0.05\ \mu m^2 \cdot s^{-1}$ and τ = 50 ms is the average time between frames. In other words, the average vesicle moves ~0.5 pixels between measurements.

The 633 nm laser exclusively excited the acceptor labels, permitting unambiguous localization of each v-SNARE vesicle. The fluorescence intensity of each individual v-SNARE vesicle, I_{red}^{633}, was determined after background-subtraction by integrating the total intensity present in a 7×7 pixel region centered at the highest-value pixel. The 514 nm laser strongly excited the donor labels in the t-SNARE vesicles, but also weakly excited the acceptor labels in the v-SNARE vesicles. The fluorescence intensity in the red and green channels during 514 nm excitation, I_{red}^{514} and I_{green}^{514}, respectively, was measured for each v-SNARE vesicle using the same region of integration as for measurement of I_{red}^{633}. The fluorescence intensity due to FRET, I_{FRET}^{514}, was determined from the measurement of I_{red}^{514} after subtracting contributions from the two major sources of cross-talk: leakage of donor (DiI) fluorescence

into the red channel and direct excitation of the acceptor label (DiD) during 514 nm excitation:

$$I_{FRET}^{514} = I_{red}^{514} - \alpha I_{green}^{514} - \beta I_{red}^{633} \quad \text{(S1)}$$

where α and β are the cross-talk correction factors. The correction factors were determined by measuring intensities for donor-only and acceptor-only vesicles and correcting to zero FRET intensity. For our system, α = 0.16 and β was determined daily to account for differences in laser alignment and intensities.

FRET efficiencies are calculated for the subset of v-SNARE vesicles that were co-localized with a donor vesicle using the equation:

$$E = \frac{\mathrm{I}_{\mathrm{FRET}}^{514}}{\mathrm{I}_{\mathrm{FRET}}^{514} + \gamma I_{green}^{514}} \quad \text{(S2)}$$

Here γ is a detection sensitivity factor that places DiI fluorescence collected in the green channel on the same scale as DiD fluorescence collected in the red channel. Co-localization includes both cases for which a donor vesicle emits green fluorescence in the same position as a v-SNARE vesicle and cases for which there is a significant amount of intensity from FRET. The second criterion finds vesicle pairs for which green fluorescence is not detected because of highly efficient FRET.

Vesicles containing both 1% DiD + 1% DiI were used to determine γ because these vesicles contain equal amounts of donor and acceptor labels and undergo almost complete FRET (E = 0.9). We first measured I_{FRET}^{514} for vesicles with high FRET, and then selectively bleached the acceptor labels using 633 nm. We then measured I_{green}^{514} using the same 514 nm laser power and image acquisition settings as for I_{FRET}^{514}. For both measurements DiI was excited at the same rate and fluorescence was collected for the same amount of time, so the ratio of the two intensities gave us γ, the relative detection efficiency for DiD fluorescence in the red channel versus DiI fluorescence in the green channel. Averaging over hundreds of vesicles gave us $\gamma = 2.0 \pm 0.1$.

The vesicles containing both 1% DiD + 1% DiI were also used to determine the relative excitation efficiencies of DiD at 633 nm versus DiI excitation at 514 nm. We imaged the mixed vesicles using 633 nm and 514 nm sequentially using the same image acquisition settings for both exposures. The total fluorescence collected was determined after correcting for differences in the collection efficiency (I_{red}^{633} vs $I_{FRET}^{514} + \gamma I_{green}^{514}$) for each individual mixed vesicle. The ratio of total collected fluorescence reflected the differences in excitation efficiency of DiD with 633 nm and of DiI at 514 nm at the relative laser powers used.

Statistical Correction for False Co-localizations

Non-specific binding of t-SNARE vesicles to the imperfectly passivated surface leads to "false co-localization" events in which a t-SNARE vesicle appears to be bound to a v-SNARE vesicle but in fact is not. Uncertainty in the location of a moving vesicle and in the mapping between the red and green channels cause us to classify t-SNARE vesicles (imaged in the green channel with 514 nm excitation) located within a 7 × 7 pixel (1.25 μm × 1.25 μm) area surrounding a tethered vesicle (imaged in the red channel during 633 nm excitation) as co-localized. Such events include both false co-localizations and real events in which vesicle pairs have docked together. We estimate the number of low FRET (defined as E < 0.25) "false co-localizations" on each surface using the following statistical correction. First we assumed that non-specific binding of t-SNARE vesicles occurs with equal probability everywhere on the surface, i.e., that the number of non-specific binding events per surface area is constant. We measured the non-specific binding density (t-SNARE vesicles per μm^2) by analyzing regions of the surface lacking any v-SNARE vesicles. Any t-SNARE binding in these regions is due to non–specific interactions between the t-SNARE vesicle and the surface. For each image, we calculated the total area susceptible to low FRET false co-localizations from the total surface area co-localized with tethered

vesicles after excluding high-FRET vesicle pairs. The product of the non-specific binding density and the area susceptible to low-FRET false co-localizations yields the number of low-FRET false co-localization events in an image. To determine the number of true docked but unfused events, this estimated low-FRET false co-localization count was subtracted from the total number of low-FRET co-localization events. High-FRET co-localization events in which a v-SNARE vesicle has docked and fused with a t-SNARE vesicle *and also* experiences false co-localization with another t-SNARE vesicle presumably occur as well. For these events, the falsely co-localized green intensity will lower the apparent FRET efficiency of the docked and fused vesicle pair.

All data analysis was performed from raw images using custom computer programs written in MATLAB (The MathWorks, Natick, MA), which are freely available upon request. The programs use published peak finding strategies (http://www.physics.georgetown.edu/matlab/index.html) (8).

SUPPLEMENTAL DATA

Size Distributions of Reconstituted v-SNARE and t-SNARE Vesicles

We immobilized hundreds of DiI-labeled t-SNARE vesicles and DiD-labeled v-SNARE vesicles. Background-corrected integrated intensities were placed on a common scale by accounting for differences in the excitation and detection sensitivities (see Supplemental Methods). Histograms of the relative vesicle radii for the populations of v-SNARE and t-SNARE were obtained by taking the square root of each corrected intensity value; these are presented in Fig. S5. The common radius scale is relative to the mean t-SNARE vesicle radius, which is set to one. The distributions of v-SNARE and t-SNARE vesicle radii are similar overall. The mean t-SNARE vesicle radius (Fig. S5*a*) is ~110% the mean v-SNARE vesicle radius (Fig. S5*b*). For both v-SNARE and t-SNARE vesicles, ~90% of the vesicles differ in radius by a factor of two or less.

Model Calculations of FRET Efficiencies for Docked and Fully Fused Vesicle Pairs

Full fusion between a vesicle labeled with 2% donors and a vesicle labeled with 2% acceptors results in a product vesicle whose final concentrations are less than 2% and dependent on the relative surface area of the two vesicles. When two equal-sized vesicles dock and fully fuse together the product vesicle has 1% of each label in each leaflet.

Here we calculate the range of FRET efficiency values expected for a docked and fully fused vesicle pair with each vesicle labeled at 2% with DiI or DiD. Because FRET efficiency falls off rapidly with distance, we modeled each vesicle lipid bilayer as two infinite parallel planes. Each plane contains a random distribution of donors and acceptors. The model assumes that the positions of the labels do not change, that there is no excitation transfer between donor labels, and that R_0 is the same for all donor-acceptor pairs. When these assumptions are met, the infinite plane model geometry accurately predicts the FRET efficiency of donors present in the same membrane as acceptors in small (~28 nm diameter) lipid vesicles (9).

Donors undergo FRET to acceptors with an efficiency E that can be determined using (9):

$$E = 1 - \frac{1}{\tau_0}\int_0^\infty e^{-t/\tau_0} e^{-\sigma S(t)} dt \qquad \text{(S3).}$$

For our infinite parallel plane geometry, σ is the surface density of acceptor labels in labels/nm^2, τ_0 is the characteristic fluorescence lifetime of the donor labels in the absence of FRET, and $S(t)$ has two terms, one for each plane containing a random distribution of acceptors. The first term is from acceptors in the same plane as the donors where the distance of closest approach (lower limit of the integral) between the labels is a, the center-to-center distance between labels. The second term represents the parallel plane containing acceptors that is separated by a distance h from the donor plane,

$$S(t) = \int_a^{\infty} \left[1 - e^{-\left(t/\tau_0\right)\left(R_0/r\right)^6} \right] 2\pi r dr + \int_h^{\infty} \left[1 - e^{-\left(t/\tau_0\right)\left(R_0/r\right)^6} \right] 2\pi r dr \quad \text{(S4)}.$$

R_0 is the Förster radius of the FRET pair. To estimate the R_0 of the DiI-DiD FRET pair, we collected an absorption spectrum $\varepsilon_A(\lambda)$ for DiD and a fluorescence emission spectrum $F_D(\lambda)$ for DiI and inserted these into the standard equation (10):

$$R_0^6 = \frac{9000(\ln 10)\kappa^2 \phi_D}{128\pi^5 N_A n^4} \int_0^{\infty} F_D(\lambda)\varepsilon_A(\lambda)\lambda^4 d\lambda \quad \text{(S5)}$$

Here N_A is Avogadro's number, n is the index of refraction, ϕ_D is the donor fluorescence quantum yield, and κ^2 is the orientation factor. We assumed that the donor and acceptor transition dipoles are confined to a common plane, in which case $\kappa^2 = 2$ (11). The range of literature values for the DiI fluorescence quantum yield is 0.07-0.21 (12, 13), corresponding to R_0 = 5.4–6.5 nm.

We used Mathcad (Parametric Technology Corporation, Needham, MA) to numerically integrate Eqs. S3 and S4 and calculate E vs the percentage of acceptor labels in the membrane. We assumed that each lipid or label occupies 0.65 nm^2 of surface area (σ = *% acceptors* · 0.015 nm^{-2}). The value used as the distance of closest approach between labels was our estimate for the average center-to-center distance between lipids (a = 0.84 nm) and the distance between planes was our estimate for the thickness of a lipid bilayer (h = 4 nm). The results are presented in Fig. S6 for R_0 = 5, 6, and 7 nm.

We experimentally tested these models by reconstituting vesicles with a range of DiI and DiD concentrations. We used three different acceptor concentrations: 0.1%, 0.33%, and 1% DiD with DiI (the donor) at two different concentrations for each acceptor concentration. The specific "high donor" mixtures were: 0.1% DiD + 1.9% DiI, 0.33% DiD + 1.67% DiI, 1% DiD + 1% DiI, and "low donor" mixtures were: 0.1% DiD + 0.48% DiI, 0.33% DiD + 0.42% DiI, and 1% DiD + 0.25% DiI. We measured the FRET efficiencies of hundreds of immobilized vesicles for each of the 6 labeling mixtures (Eq. S2 and Methods). The mean experimental FRET efficiency values are plotted in Fig. S6 vs the percentage of acceptors. The experimental FRET efficiency values agree reasonably well with our models for R_0 = 5-7 nm, which lends support to the calculations. Importantly, the FRET efficiency values at a given acceptor concentration agree to within ~20% when the donor concentrations are varied a factor of four (Fig. S6), which argues against significant excitation transfer among donors (homoFRET).

Calculated FRET Efficiencies for Docked but Unfused Vesicle Pairs

Docked but unfused vesicles were modeled as a pair of touching spheres. Each sphere has two surfaces ("lipid bilayer leaflets") that are separated by 4 nm and decorated with a random distribution of labels. A coordinate for each label was generated by assigning a random azimuthal angle (sampled from a uniform distribution) and a random polar angle (sampled from a cosine distribution) using MATLAB.

We then used the label coordinates to calculate a Förster transfer rate for each donor label. First we calculated a list of distances $r_{D_j - Acc_i}$ between the position of donor j and each of the N_{Acc} acceptor labels. We used these distances to calculate the final transfer rate from that particular donor label to each of the acceptor labels, assuming the rate follows the distance dependence expected from Förster theory. The sum of the parallel rates gives us the transfer rate k_{T,D_j} from each donor (14):

$$k_{T,D_j} = \frac{1}{\tau_0} \sum_{i=1}^{N_{Acc}} \left(\frac{R_0}{r_{D_j - Acc_i}} \right)^6 \quad \text{(S6)}$$

where R_o is the Förster radius and τ_0 is the donor's lifetime in the absence of acceptors. The FRET efficiency of each donor j is calculated from:

$$E_{D_j} = \frac{k_{T,D_j}}{k_{T,D_j} + k_{rad} + k_{nr}} = \frac{\sum_{i=1}^{N_{Acc}} \left(\frac{R_0}{r_{D_j - Acc_i}} \right)^6}{\sum_{i=1}^{N_{Acc}} \left(\frac{R_0}{r_{D_j - Acc_i}} \right)^6 + 1} \quad \text{(S7)}$$

where $\tau_0 = (k_{rad} + k_{nr})^{-1}$ is the donor fluorescence lifetime in the absence of FRET.

The linear laser polarization and the distribution of orientations of absorption transition dipoles on the donor vesicle surface makes an inhomogeneous distribution of donor excitation efficiency. The experiment uses the lipophilic dye DiI as the donor label. When DiI partitions into a lipid bilayer its absorption transition dipole moment preferentially orients parallel to the bilayer surface (15). To estimate the FRET efficiency of docked but unfused pairs excited by linearly polarized light, we must account for preferential excitation of DiI molecules whose transition dipoles lie parallel to the polarization axis. The probability of absorption is proportional to the square of the cosine of the angle between the donor absorption transition dipole and the electric field vector $\boldsymbol{E}$ (10). Here we estimate the relative excitation efficiency for donor labels of different orientation by making the following simplifying assumptions: the vesicles are spherical, all DiI transition dipoles are aligned parallel to the vesicle surface, the evanescent wave is s-polarized such that $\boldsymbol{E}$ has only an x-component, and the transition dipoles sample all orientations within the plane of the bilayer uniformly. We also assume that the fluorescence collection efficiency does not depend on the donor orientation, which has been shown to be a reasonable assumption for collection of fluorescence within 500 nm of the glass coverslip using a high numerical aperture objective (16).

In our models each donor transition dipole moment is located at a position on the vesicle specified by spherical polar coordinates (r, θ, ϕ) (Fig. S7*a*). Its transition dipole moment vector $\boldsymbol{d}$ lies tangent to the vesicle surface, in the $\theta\phi$-plane. We define ω as the angle $\boldsymbol{d}$ makes with $\hat{\boldsymbol{\theta}}$ in the $\theta\phi$-plane (Fig. S7*a*). We express $\boldsymbol{d}$ in terms of its projections along $\hat{\boldsymbol{\theta}}$ and $\hat{\boldsymbol{\phi}}$, local unit vectors pointing in the direction of increasing $\hat{\boldsymbol{\theta}}$ and $\hat{\boldsymbol{\phi}}$, respectively (Fig. S7*a*):

$$\boldsymbol{d} = d\cos\omega\hat{\boldsymbol{\theta}} + d\sin\omega\hat{\boldsymbol{\phi}} \quad \text{(S8)}$$

We then expand $\hat{\boldsymbol{\theta}}$ and $\hat{\boldsymbol{\phi}}$ in terms of the original Cartesian (xyz) coordinate system:

$$\hat{\boldsymbol{\theta}} = (\cos\theta\cos\phi)\hat{\boldsymbol{x}} + (\cos\theta\sin\phi)\hat{\boldsymbol{y}} - (\sin\theta)\hat{\boldsymbol{z}} \quad \text{(S9a)}$$

$$\hat{\boldsymbol{\varphi}} = (-\sin\phi)\hat{\boldsymbol{x}} + (\cos\phi)\hat{\boldsymbol{y}} \quad \text{(S9b)}$$

which gives:

$$\boldsymbol{d} = (d\cos\omega\cos\theta\cos\phi - d\sin\omega\sin\phi)\hat{\boldsymbol{x}} + (d\cos\omega\cos\theta\sin\phi + d\sin\omega\cos\phi)\hat{\boldsymbol{y}} - (d\cos\omega\sin\theta)\hat{\boldsymbol{z}} \quad \text{(S10).}$$

The dot product of $\boldsymbol{d}$ and $\boldsymbol{E}$ is given by $\boldsymbol{E}\cdot\boldsymbol{d} = E\,d\cos\xi$, where ξ is the angle between these two vectors. For $E = d = 1$ and $\boldsymbol{E} = \hat{\boldsymbol{x}}$,

$$\boldsymbol{E}\cdot\boldsymbol{d} = \cos\xi = \cos\omega\cos\theta\cos\phi - \sin\omega\sin\phi \quad \text{(S11).}$$

The relative excitation efficiency is proportional to $\cos^2\xi$ and we assume that ω uniformly samples all angles from 0 to 2π to obtain the relative excitation efficiency of donor j as:

$$w_{exc,D_j} = \int_0^{2\pi} (\cos\omega\cos\theta\cos\phi - \sin\omega\sin\phi)^2\, d\omega \quad \text{(S12)}$$

The FRET efficiency of a docked but unfused vesicle pair is then the weighted mean of the FRET efficiencies of all N_D donors:

$$E = \frac{\sum_{j=1}^{N_D} \mathrm{w}_{\mathrm{exc,D_j}} \cdot E_{D_j}}{\sum_{j=1}^{N_D} \mathrm{w}_{\mathrm{exc,D_j}}} \quad \text{(S13).}$$

We used our best estimate for the Förster radius ($R_0 = 6$) to calculate the FRET efficiency E for pairs of docked but unfused vesicles labeled at 2%. The FRET efficiency depends on the orientation of the vesicles relative to $\boldsymbol{E}$ (Fig. S7*c*, *d*). In Fig. S7*e* we present FRET efficiencies for modeled pairs of docked but unfused vesicles with donor radius R_D and acceptor radius R_A that sample many vesicle pair orientations. The vesicle pairs sample 11 different values of α in the range 0–90º (0, 9º…90º); for each α the pair samples 11 different values of β (0, 36º…360º). The average value of E at each α comes from equal weighting of the values obtained for each β. The final orientationally averaged FRET efficiencies are presented in Fig. S7*e*. These results average the E values obtained at each α with sinα weighting to mimic a uniform distribution of orientations over a hemisphere. As shown, very small t-SNARE vesicles ($R_D = 15$ nm), which are rare, have FRET efficiencies in the range 0.12–0.22. Average-sized t-SNARE vesicles (25 nm < R_D < 50 nm) that are docked but unfused always have $E < 0.10$, and often much smaller. Large t-SNARE vesicles ($R_D > 50$ nm) paired with any size acceptor vesicle always have $E < 0.05$. Our modeling shows that for the vast majority of docked but unfused vesicle pairs $E < 0.25$ and that exciting the donors with s-polarized light slightly enhances the mean FRET efficiency as compared with the case of donors that are uniformly excited (Fig. S7 *f*).

Determination of a FRET Efficiency Threshold

Next we calculate the probability that a vesicle *fusion* product would have $E < 0.25$ and potentially be confused with vesicle pairs in the docked but unfused state. Figure S6 shows that $E < 0.25$ occurs when a fused vesicle pair contains < 0.2% DiD. This would require that a t-SNARE vesicle dock and fuse with a v-SNARE vesicle with nine times less surface area. Assuming random pairing between our vesicles (Fig. S5), such a pairing would occur < 2% of the time. For the remaining > 98% of vesicle pairs full fusion will result a vesicle with > 0.2% DiD, and therefore $E > 0.3$. Modeling docked but unfused pairs suggests that for the vast majority of pairs $E < 0.25$ (Fig. S7). In summary, the modeling supports a cutoff of $E = 0.25$ and predicts a clean separation between populations of vesicles that are docked but unfused vs docked and fused. This threshold is supported by real time observation of single docking and fusion events (Fig. S9).

Calculated FRET Efficiencies for Docked and Hemifused Vesicle Pairs

For docked and hemifused vesicles, the hemifusion product was modeled as *two different pairs* of parallel planes with each pair spaced by 4 nm. One pair of planes models the hemifused donor vesicle while the other pair models the hemifused acceptor vesicle. The model of the hemifused donor vesicle has one plane containing 2% donor labels (to represent the unmixed donor inner leaflet) and one plane containing a mixture of donors and acceptors (to represent the mixed outer leaflet). The model of the hemifused acceptor vesicle has one plane containing 2% acceptor labels (to represent the unmixed acceptor inner leaflet) and one plane containing a mixture of donors and acceptors (to represent the mixed outer leaflet). The labeling fractions of the mixed planes is the same for both vesicles, and is determined from the ratio of donor to acceptor vesicle surface areas. We assumed that there is no FRET between vesicles, so that we expect the model to slightly underestimate E for hemifusion.

In the hemifusion model, there are three different populations of donor labels that differ in the concentration of surrounding acceptors. Each donor population has its own donor quenching term ($S(t)$ in Eq. S4), and thus different average FRET efficiency E. For the donor vesicle inner leaflet, we set the minimum intra-plane spacing between labels to infinity ($a = \infty$, because there are no acceptors in the same plane as these donors) and the minimum inter-plane spacing as the thickness of the bilayer ($h = 4$ nm). In contrast, the donor labels present in the donor vesicle outer leaflet carry out FRET only to acceptors present in the same plane ($a = 0.84$ nm and $h = \infty$). The donor labels in a hemifused acceptor vesicle outer leaflet carry out FRET to acceptors in their own plane and in the other leaflet plane

(a = 0.84 nm and h = 4 nm). For each docked and hemifused pair, the overall mean FRET efficiency E was calculated from the weighted average of the E values determined for the donors present in the three different leaflets. The results using R_0 = 6 nm are plotted in Fig. S8*b*; these can be directly compared with the results for full fusion in Fig. S8*a*.

The model predicts a wide range of FRET efficiency values, E = 0.25-1.0, arising from docked and fully fused vesicles when the donor and acceptor vesicles range in size from 15-75 nm (Fig. S5). Perhaps surprisingly, the model predicts a similar range of values, E = 0.15-0.9, arising from docked and hemifused pairs. The two FRET efficiency distributions overlap severely. For given vesicle sizes in a vesicle pair, the difference in E between the hemifused and fused states varies only from 0.1 to 0.2. For example, two 45 nm vesicles that have docked and hemifused have E = 0.8; once they fully fuse E increases only to 0.9. The difference between E for hemifusion vs full fusion is much smaller than the range of FRET efficiency values expected to arise from random pairing between vesicles with the size distribution used in this study. Therefore, we conclude that we cannot distinguish between full fusion and hemifusion using the DiI/DiD FRET pair when the vesicles are originally labeled at 2%.

SUPPLEMENTAL REFERENCES

1. Weber, T., B. V. Zemelman, J. A. McNew, B. Westermann, M. Gmachl, F. Parlati, T. H. Sollner, and J. E. Rothman. 1998. SNAREpins: Minimal machinery for membrane fusion. Cell 92:759-772.
2. Tucker, W. C., T. Weber, and E. R. Chapman. 2004. Reconstitution of Ca2+-regulated membrane fusion by synaptotagmin and SNAREs. Science 304:435-438.
3. Axelrod, D. 2001. Selective imaging of surface fluorescence with very high aperture microscope objectives. J. Biomed. Opt. 6:6-13.
4. Chen, X. C., D. Arac, T. M. Wang, C. J. Gilpin, J. Zimmerberg, and J. Rizo. 2006. SNARE-mediated lipid mixing depends on the physical state of the vesicles. Biophys. J. 90:2062-2074.
5. Liu, T. T., W. C. Tucker, A. Bhalla, E. R. Chapman, and J. C. Weisshaar. 2005. SNARE-driven, 25-millisecond vesicle fusion in vitro. Biophys. J. 89:2458-2472.
6. Wang, T. T., E. A. Smith, E. R. Chapman, and J. C. Weisshaar. 2009. Lipid Mixing and Content Release in Single-Vesicle, SNARE-Driven Fusion Assay with 1-5 ms Resolution. Biophys. J. 96:4122-4131.
7. Kapanidis, A. N., N. K. Lee, T. A. Laurence, S. Doose, E. Margeat, and S. Weiss. 2004. Fluorescence-aided molecule sorting: Analysis of structure and interactions by alternating-laser excitation of single molecules. Proc. Natl. Acad. Sci. U. S. A. 101:8936-8941.
8. Crocker, J. C., and D. G. Grier. 1996. Methods of digital video microscopy for colloidal studies. J. Colloid Interface Sci. 179:298-310.
9. Fung, B. K. K., and L. Stryer. 1978. SURFACE DENSITY DETERMINATION IN MEMBRANES BY FLUORESCENCE ENERGY-TRANSFER. Biochemistry 17:5241-5248.
10. Lakowicz, J. R. 2006. Principles of Fluorescence Spectroscopy. Springer, New York, NY.
11. Gullapalli, R. R., M. C. Demirel, and P. J. Butler. 2008. Molecular dynamics simulations of DiI-C-18(3) in a DPPC lipid bilayer. Phys. Chem. Chem. Phys. 10:3548-3560.
12. Sims, P. J., A. S. Waggoner, C. H. Wang, and J. F. Hoffman. 1974. STUDIES ON MECHANISM BY WHICH CYANINE DYES MEASURE MEMBRANE-POTENTIAL IN RED BLOOD-CELLS AND PHOSPHATIDYLCHOLINE VESICLES. Biochemistry 13:3315-3330.
13. Tsien, R. a. W., A. 1995. Fluorophores for Confocal Microscopy: Photophysics and Photochemistry.
14. Förster, T. 1948. Intermolecular energy migration and fluorescence. Ann. Phys 2:55-75.
15. Axelrod, D. 1979. CARBOCYANINE DYE ORIENTATION IN RED-CELL MEMBRANE STUDIED BY MICROSCOPIC FLUORESCENCE POLARIZATION. Biophys. J. 26:557-573.

16. Anantharam, A., B. Onoa, R. H. Edwards, R. W. Holz, and D. Axelrod. Localized topological changes of the plasma membrane upon exocytosis visualized by polarized TIRFM. J. Cell Biol. 188:415-428.